LU TP 99–43
September 2000
Revised

Minijets and Transverse Energy Flow in High Energy Collisions

Gösta Gustafson[1] and Gabriela Miu[2]

Department of Theoretical Physics,
Lund University, Lund, Sweden

Abstract

When studying the production of minijets and transverse energy flow in high energy hadron-hadron or nucleus-nucleus collisions, two essential points have to be taken into account. First, one has to account for the virtuality of the colliding partons and secondly, it is important to avoid double counting, when many links in a parton chain can be interpreted as the momentum transfer in a hard subcollision. The Linked Dipole Chain model, introduced for low-x DIS, is particularly suitable for a study of these problems. It describes (mini)jet production in a $k_\perp$-factorizing formalism, which includes all links in a parton chain on an equal footing, avoiding double counting. In a "naive" calculation based on integrated structure functions, the cross section blows up for small $p_\perp$, which makes it necessary to introduce a soft cutoff. In our approach we find a dynamical suppression at low $p_\perp$, which makes it possible to extrapolate to higher energies and make more reliable predictions for RHIC and LHC.

[1]gosta@thep.lu.se
[2]gabriela@thep.lu.se

1 Introduction

With increasing energies in hadron-hadron or nucleus-nucleus collisions, the cross section for hard subcollisions increases and becomes more and more important. The amount of minijets and transverse energy becomes essential for understanding the background in searches for new particles or new phenomena at the LHC as well as for the "initial conditions" in nucleus-nucleus collisions. In calculations of the flow in either a quark-gluon plasma or a hadronic phase, the results are very sensitive to the properties of the initial parton state which resulted from a large number of hard subcollisions. Thus a reliable estimate of these initial conditions is essential for the interpretation of signals from a possible plasma formation in experiments at RHIC or LHC.

At high $q_\perp$ the jet cross section can be described by a product of structure functions describing the flux of partons and the cross section for a hard partonic subcollision. Symbolically we write (cf. Fig. 1a)

$$\frac{d\sigma}{dq_\perp^2} \sim F(x_1, q_\perp^2)\, F(x_2, q_\perp^2)\, \frac{d\hat{\sigma}}{dq_\perp^2}. \tag{1}$$

This is a relevant description when $q_\perp$ is so large that the structure functions can be described by DGLAP evolution, i. e. by $k_\perp$-ordered chains from the incoming hadrons towards the hard subcollision. In the hard collision cross section, $d\hat{\sigma}/dq_\perp^2$, the colliding partons are then approximately on shell. For smaller $q_\perp^2$ and/or larger energies (which implies smaller x-values) we enter the BFKL region, in which non-ordered chains are important. This has two essential consequences:

i) The virtuality of one or both of the colliding partons ($k_{\perp 1}^2$ and/or $k_{\perp 2}^2$ in Fig. 1a) can be larger than the momentum transfer $q_\perp^2$. This implies that the virtualities of the colliding partons have to be taken into account. This can be achieved by means of nonintegrated structure functions and off-shell subcollision cross sections.

ii) In a chain with non-ordered $k_\perp$-values a single hard subcollision cannot be isolated. There may be several links in a single chain, which can be regarded as a hard collision. This situation can be analyzed in a formalism in which every link in Fig. 1 can be regarded as a hard subcollision. This implies that each final state parton is active in two different subcollisions. (The number of links in the chain determines both the number of subcollisions and the number of final state partons.) Therefore special care has to be taken to avoid double counting.

A formalism for DIS which interpolates between the DGLAP and BFKL regions, and which describes both the cross section and the final state properties, was developed by Ciafaloni, Catani, Fiorani, and Marchesini [1]. This or equivalent formalisms can be used e. g. to calculate the production of heavy quarks in hadronic collisions. In this reaction there is a single link which contains the heavy quark, and the CCFM formalism or the semihard approach can be used to calculate the unordered evolution towards the heavy quark from the projectile and the target ends [2]. Thus these formalisms can be used to solve problem i) above.

For non-$k_\perp$-ordered chains the single diagram in Fig. 1 can correspond to many hard subcollisions, e. g. $1 + 2 \to 3 + 4$ and $5 + 6 \to 7 + 8$ in Fig. 1b. For the first reaction, $1 + 2 \to 3 + 4$, the section of the ladder between partons 2 and 5 should be regarded as an evolution from the top (projectile) end, while for the reaction 5+6 $\to$ 7+8 the same section should be regarded as an evolution from the lower (target) end of the chain. A description of this process is most simple in a formalism in which the evolution is explicitly symmetric

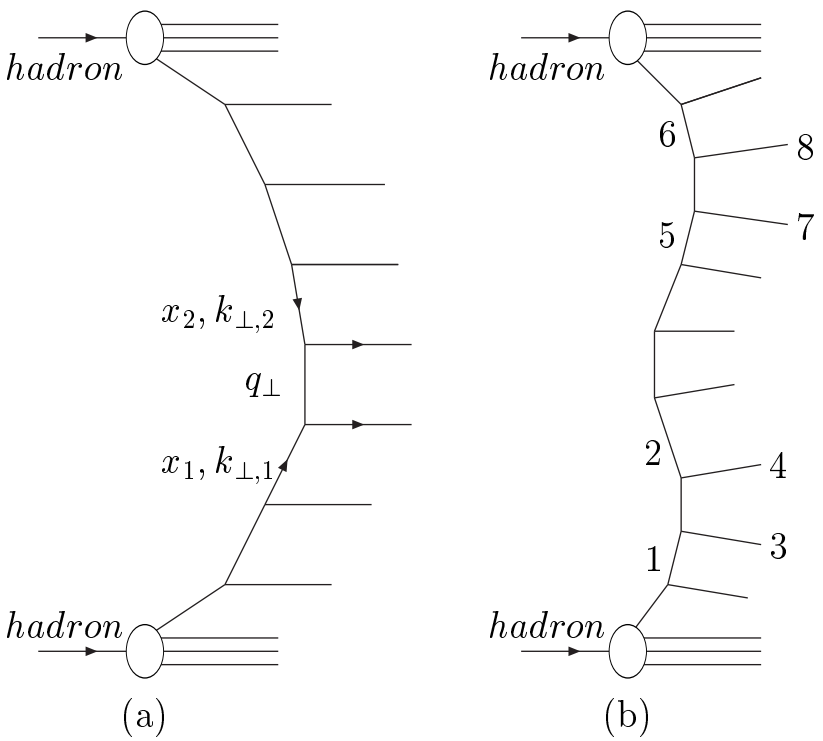

Figure 1: *A fan diagram for a hadron-hadron collision.*

between the two ends. It is also essential that the formalism can be interpreted in terms of production probabilities for exclusive final states. The symmetry is not a trivial feature for the following reason. The fan diagrams in Fig. 1 should be regarded as the initial state radiation. To get the complete final state, final state emission has to be added in specified kinematic regions. The separation between initial state and final state emission is not determined by Nature, but is defined by the calculation scheme, and therefore the regions for final state emission depend on the formalism used. In the CCFM approach this separation is not symmetric, and consequently also the initial state ladder is asymmetric. Thus the CCFM formalism is not immediately convenient to describe many subcollisions in a single chain, and thus to solve problem ii) above.

The final state emission, when one gluon is split into two, should not significantly affect the flow of energy. Note, however, that the distribution of produced gluons is not a uniquely defined quantity. Besides the arbitrariness in the separation between initial and final state emission, discussed above, also the final state radiation depends on the resolution chosen in the definition of an individual gluon, i. e. on the cut-off in the final state cascades.

The Linked Dipole Chain (LDC) model [3, 4] is a reformulation and generalization of the CCFM formalism. The separation between initial and final state radiation is chosen in such a way that the description is explicitly symmetric between the projectile and target ends of the ladder. It can within a single formalism describe different types of events, "normal DIS", boson-gluon fusion events, and events with hard subcollisions in resolved photon events. For such a resolved photon event the result can be directly interpreted as evolutions from both the proton and the photon ends towards a hard parton-parton collision. This feature implies that the LDC model is also particularly suitable for a description of hard collisions in hadronic interactions. For any link in the ladder, the contribution can be directly interpreted as evolution from the two ends multiplied by an

off-shell parton-parton cross section for the link under study. This symmetry property of the LDC model makes it useful in solving problem ii) above (the double-counting is easily corrected for in this formalism).

It is well known that the BFKL formalism with a constant coupling, α_s, implies that the transverse momenta grow like a random walk in y or in $\ln 1/x$ (what is called Bartels' cigar). For a running α_s we obtain instead a saturation of the $k_\perp$-distribution [4]. Therefore very large chains develop a central plateau in rapidity. This means that with increasing beam energy the transverse energy density in each chain will stay limited, although the total $dE_\perp/dy$ will increase as the number of possible chains grows with energy. The fact that the $k_\perp$-distribution stays limited also for high energies implies that the result is sensitive to soft nonperturbative physics, and thus depends on a necessary cut-off for small $k_\perp$. This cut-off can, however, be fixed by a phenomenological fit to experimental data for $F_2(x, Q^2)$, and therefore does not imply a large extra uncertainty.

When comparing our result with the "naive" expression in eq. (1) we find that the latter significantly overestimates the cross section for smaller $q_\perp$. In order to agree with experimental data for $E_\perp$-flow, many calculations based on eq. (1) introduce a cutoff for small $q_\perp$ of the order 2 GeV/c [5]. This implies, however, that it is difficult to make predictions for higher energies. Without a dynamical understanding of the origin of the overestimate, it is not possible to judge how an effective cut-off should vary with energy. The dynamical suppression in our formalism corresponds to such an effective cut-off, indeed of the order 2 GeV/c, which is growing slowly with the total collision energy.

The results in this paper are mainly based on approximate analytic calculations, which demonstrate the qualitative features. In a future publication we want to present more detailed results based on MC simulations, where e. g. corrections from quark lines, subleading terms in the splitting functions and exact energy-momentum conservation, are also taken into account.

2 DIS

A deep inelastic scattering event is generally described in terms of a fan diagram as shown in Fig 2. Here q_i denote quasireal partons emitted as initial state radiation, while the links k_i are virtual. The dashed lines denote final state emission, which is assumed to be emitted without changing the cross section and with negligible recoils for the emitting partons q_i.

In the large Q^2 region, the DGLAP region, the dominant contributions come from ordered chains which satisfy $Q^2 > k^2_{\perp,n} > ... > k^2_{\perp,i} > k^2_{\perp,i-1}$ and $k_{+,i} > k_{+,i+1}$. Each such chain gives a contribution ($x_i \equiv k_{+,i}/P_{+,tot}$)

$$\prod_i^n \bar{\alpha} \frac{dx_i}{x_i} \frac{dk^2_{\perp,i}}{k^2_{\perp,i}} \quad \text{where} \quad \bar{\alpha} \equiv \frac{3\alpha_s}{\pi}. \tag{2}$$

Integrating over the appropriate integration regions and summing over possible values of n, the number of links in the chain, we readily obtain (for a fixed coupling $\bar{\alpha}$)

$$F(x, Q^2) \sim \sum_n \bar{\alpha}^n \frac{(\ln 1/x)^n}{n!} \frac{(\ln Q^2)^n}{n!} \approx \exp(2\sqrt{\bar{\alpha} \ln Q^2 \ln 1/x}). \tag{3}$$

For a running coupling we get instead of $\ln Q^2$ a factor $\ln \ln Q^2$. We want to stress that to get the properties of the *final state*, we have to add final state emission within regions allowed by angular ordering.

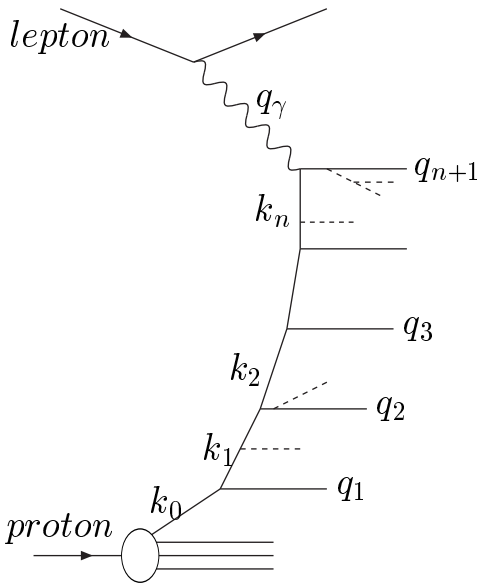

Figure 2: *A fan diagram for a DIS event. The quasireal partons from the initial state radiation are denoted q_i, and the virtual propagators k_i. The dashed lines denote final state radiation.*

For very small x and limited Q^2, the BFKL region, also non-ordered chains become important, although suppressed. Solutions to the BFKL equation [6] increase like a power $1/x^\lambda$ for small x-values. Such a power-like behavior with $\lambda \sim 0.3$, is indicated in data on F_2 from HERA. (We note, however, that it is also possible to describe this increase by NLO DGLAP evolution.)

In the interpolation region between the DGLAP and BFKL regimes we have to calculate suppressed contributions from non-ordered chains. For each chain of initial state radiation, final state emission should be added within specified kinematic regions. This final state radiation should give negligible recoils. It should also be described by Sudakov form factors, which implies that the final state emission only affects the properties of the final state and not the cross section (i. e. the reaction probability), which is described by the structure function. Thus a chain with specified initial state radiation represents a set of final states with all possible final state emissions within the allowed regions. We want to stress that the separation between initial and final state radiation is not given by Nature, but is defined by the calculation scheme.

A specific scheme, which interpolates between the DGLAP and the BFKL results, was presented by Ciafaloni, Catani, Fiorani and Marchesini, the CCFM model [1]. In this scheme those final state gluons, which are not followed in rapidity (or angle) by a more energetic gluon, are regarded as initial state radiation, all other as final state emission. With this definition they showed that for small x the nonintegrated structure function, f, is given by the expression (see ref [1] for details)

$$f(x,k_\perp^2,q^2) \sim \sum_n \int \prod^n \bar{\alpha}\frac{dz_i}{z_i}\frac{d^2q_{\perp,i}}{\pi q_{\perp,i}^2}\Delta_{ne}(z_i,k_{\perp,i}^2,q_i^2)\delta(x-\Pi z_i)\delta(k_\perp^2-k_{\perp,n}^2)\delta(q^2-q_n^2). \quad (4)$$

Here $q_{\perp,i}$ and $k_{\perp,i}$ are the transverse momentum of the real and virtual partons as indicated in Fig. 2, and the variable q is defined by the relation $q \equiv q_\perp/(1-z)$, and the function

$\Delta_{ne}(z, k_\perp^2, q^2)$ is a specific non-eikonal form factor. The integration region is restricted by the relation

$$q_{\perp,i+1} > z_i q_{\perp,i}/(1-z_i) \tag{5}$$

which follows from angular ordering, and by the kinematic constraint (called the consistency constraint)

$$k_{\perp,i}^2 > z_i q_{\perp,i}^2. \tag{6}$$

We note that this nonintegrated structure function $f(x, k_\perp^2, q^2)$ depends on two scales, $k_\perp$ which defines the transverse momentum of the last link in the chain, and q which depends on the angle of the last emission, and therefore specifies the boundary of the angular region in which later emissions are allowed.

3 The Linked Dipole Chain Model

The Linked Dipole Chain model [3] (LDC) is a reformulation and generalization of the CCFM model. In the LDC model more gluons are treated as final state radiation. The remaining (initial state) gluons are ordered both in q_+ and in q_-. (This implies that they are also ordered in angle or rapidity y.) Thus a single chain in the LDC model represents a set of chains in the CCFM scheme, all with the same "backbone" of harder gluons. In ref [3] it is demonstrated that if we sum over all states in this set, with their corresponding non-eikonal form factors, then all this adds up to unity. Thus the form factors are exactly canceled, and a nonintegrated structure function $\mathcal{F}$ can be written in the simple form

$$\mathcal{F}(x, k_\perp^2) \sim \sum_n \int \prod^n \bar{\alpha} \frac{dz_i}{z_i} \frac{d^2 q_{\perp,i}}{\pi q_{\perp,i}^2} \theta(q_{+,i-1} - q_{+,i}) \theta(q_{-,i} - q_{-,i-1}) \delta(x - \Pi z_i) \delta(\ln k_\perp^2 - \ln k_{\perp,n}^2). \tag{7}$$

We note in particular that this result is symmetric in q_+ and q_-. (An essential point for this symmetry and the cancelation of the non-eikonal form factors is the consistency constraint in eq. (6).) The fact that the ordering in both q_+ and q_- also automatically implies an ordering in y (i. e. in angle), means that the nonintegrated structure function $\mathcal{F}(x, k_\perp^2)$ depends only on *one* scale, $k_\perp^2$. (In contrast, the corresponding form factor, $f(x, k_\perp^2, q^2)$, in the CCFM model also depends on the scale q^2, related to the boundary of the angular region allowed for further emissions.) This fact implies a considerable simplification of the formalism. The symmetry also implies that the chain in Fig 2 can be interpreted either as evolving from bottom to top (i. e. from the proton end towards the photon) or evolving from top to bottom (from the photon towards the proton). This feature will be essential for our analysis of the minijet distribution.

Fig. 3 shows a typical chain in a $(y, \ln q_\perp^2)$-plane. The real emitted partons q_i are mapped onto points in this figure. The lightcone components $\ln q_\pm = \pm y + \frac{1}{2} \ln q_\perp^2$ grow in the upper right and upper left directions as indicated in the figure. The virtual propagators do not have a well defined rapidity; they are represented by horizontal lines, whose left ends correspond to the values of $k_{\perp,i}$ and $k_{+,i}$, while the right ends correspond to $k_{\perp,i}$ and $k_{-,i}$. The larger region allowed for final state radiation in the LDC model corresponds to the region below the horizontal lines in Fig. 3.

It is convenient to express the result in terms of the propagator momenta k_i, using the relations $d^2 q_{\perp,i} = d^2 k_{\perp,i}$ and $q_{\perp,i}^2 \approx \max(k_{\perp,i}^2, k_{\perp,i-1}^2)$. Thus eq. (7) can be written in the form

$$\mathcal{F} \sim \sum \int \prod \bar{\alpha} \frac{dz_i}{z_i} \frac{dk_{\perp,i}^2}{\max(k_{\perp,i}^2, k_{\perp,i-1}^2)}. \tag{8}$$

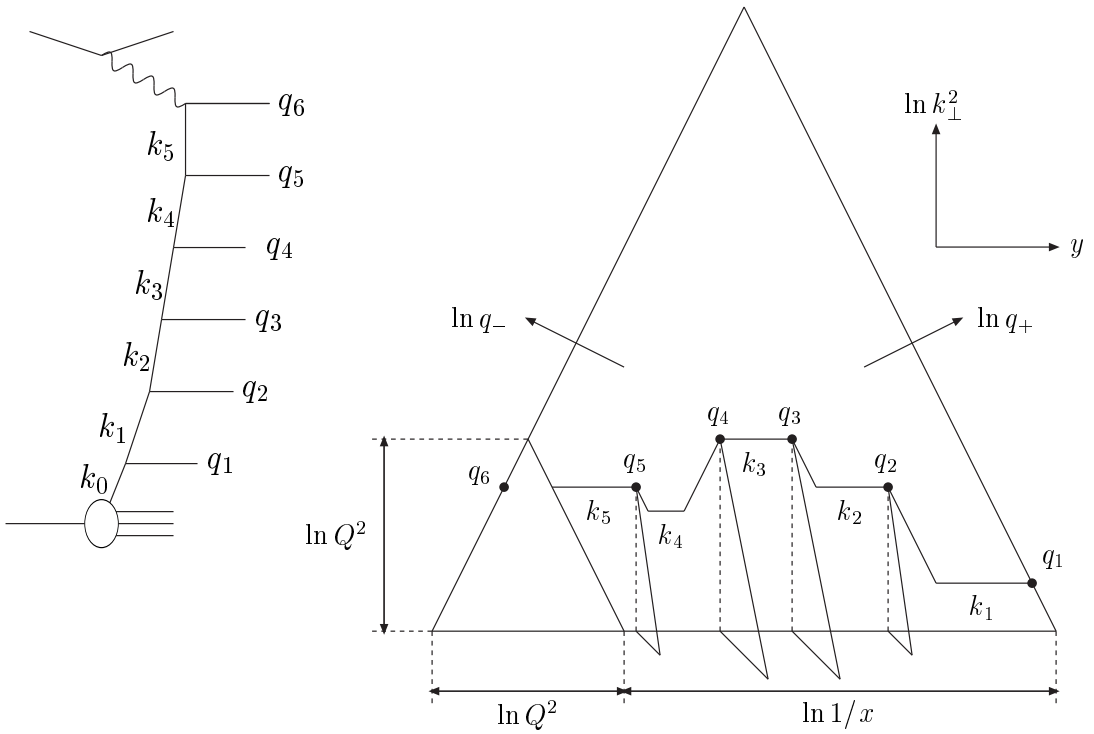

Figure 3: *The initial state emissions q_i in the $(y, \kappa = ln(k_\perp^2))$-plane. Final state radiation is allowed in the region below the horizontal lines.*

where we have suppressed the θ- and δ-functions. This result implies that for a "step up" or a "step down" in $k_\perp$ we find the following weights

$$\frac{d^2q_{\perp,i}}{q_{\perp,i}^2} \approx \frac{d^2k_{\perp,i}}{k_{\perp,i}^2}, \quad k_{\perp,i} > k_{\perp,i-1} \quad \text{and} \tag{9}$$

$$\frac{d^2q_{\perp,i}}{q_{\perp,i}^2} \approx \frac{d^2k_{\perp,i}}{k_{\perp,i}^2} \cdot \frac{k_{\perp,i}^2}{k_{\perp,i-1}^2}, \quad k_{\perp,i} < k_{\perp,i-1}. \tag{10}$$

Thus for a step down we have an extra suppression factor $k_{\perp,i}^2/k_{\perp,i-1}^2$. This implies that if the chain goes up to $k_{\perp,max}$ and then down to $k_{\perp,final}$ we obtain the factor

$$\prod \frac{dk_{\perp,i}^2}{k_{\perp,i}^2} \cdot \frac{k_{\perp,final}^2}{k_{\perp,max}^2}. \tag{11}$$

This gives a factor $1/k_{\perp,max}^4$, which corresponds to a hard parton-parton subcollision.

In DIS also chains for which $k_{\perp,final}^2 > Q^2$ can contribute to the cross section. These chains correspond to boson-gluon fusion events, and the definition of the structure function $F(x,Q^2)$ implies that these contributions contain a similar suppression factor $Q^2/k_{\perp,final}^2$. Thus the relation between the integrated and the nonintegrated structure functions, sometimes symbolically written as $F(x,Q^2) \sim \int \frac{dk_\perp^2}{k_\perp^2}\mathcal{F}(x,k_\perp^2)$, is more explicitly given by the relation

$$F(x,Q^2) = \int^{Q^2} \frac{dk_\perp^2}{k_\perp^2}\mathcal{F}(x,k_\perp^2) + \int_{Q^2} \frac{dk_\perp^2}{k_\perp^2}\mathcal{F}(x\frac{k_\perp^2}{Q^2},k_\perp^2)\frac{Q^2}{k_\perp^2}. \tag{12}$$

In the second term, besides the suppression factor $Q^2/k_\perp^2$ we have also a shifted x-value. ' 'Normal" chains, for which $k_{\perp,final}^2 < Q^2$, end on the line AB in Fig. 4, which corresponds

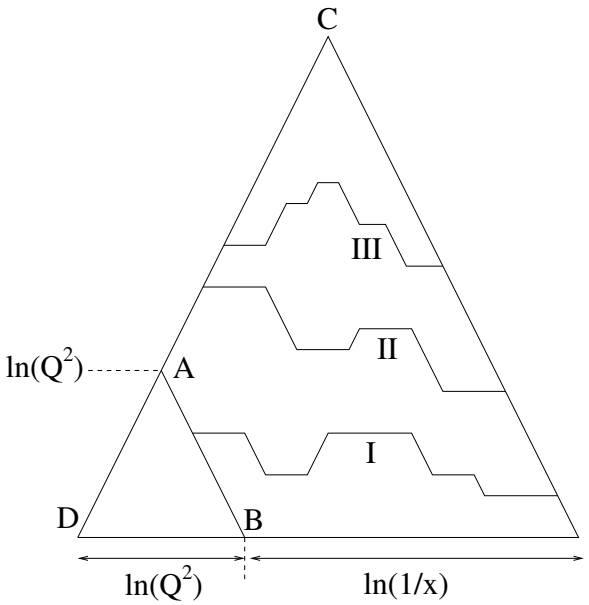

Figure 4: *Different types of parton chains. I: "Normal" DIS. II: Boson-gluon fusion. III: Hard resolved photon collision.*

to $k_{+,final} = x \cdot P_{+,tot}$, but due to energy-momentum conservation, chains for which $k^2_{\perp,final} > Q^2$ end instead on the line AC, which corresponds to $k_{+,final} = x \cdot \frac{k^2_{\perp,final}}{Q^2} \cdot P_{+,tot}$. Note that the relation in eq. (12) is a leading approximation valid when $k^2_\perp$ is either much smaller or much larger than Q^2. Exact energy-momentum conservation implies that the argument in $\mathcal{F}$ should be $x(k^2_\perp + Q^2)/Q^2$, which approaches x or $xk^2_\perp/Q^2$ in the two limits. The exact kinematic relation is included in the MC in the whole chain including this final vertex. Our experience indicates that the approximations presented here are sufficient to understand the essential properties.

We see that in the LDC model different types of reactions are treated in the same formalism, without double counting or missed parts of phase space. Thus Fig. 4 shows three chains representing different types of reactions:

I. "normal" DIS,

II. boson-gluon fusion: $k^2_{\perp,final} > Q^2$,

III. hard resolved photon collision: $k^2_{\perp,max} > k^2_{\perp,final} (> Q^2)$.

As mentioned above, the LDC formalism is fully *left-right symmetric*, meaning that the same result is obtained if the chain is generated from the photon end instead of from the proton end. Although not evident from eq. (8), this is obvious from the expression in eq. (7). This feature also means that the same formalism can be used if the (resolved) photon in one end of the chain is replaced by a hadron. In section 5 we will see that the symmetric property of the LDC formalism makes it particularly effective for an understanding of the minijet distribution in hadronic reactions or nucleus-nucleus collisions. It is also important that the result in eq. (7) not only describes inclusive properties, but can be interpreted as the production probability for an exclusive final state.

Before we go into more details about the properties of this minijet plateau, we want to mention some other properties of the LDC model:

- It is straight forward to allow for a running coupling α_s within the formalism.

- It is possible to include quarks and other non-leading effects (non-leading terms in the splitting functions and exact energy-momentum conservation). The result is also improved when the link with highest $p_\perp$ is adjusted to the exact matrix element.

- The chains contain only those gluons (or quarks), which cannot be regarded as final state radiation. This might be called the "backbone" of the chain, and the fact that hard jets are not yet subdivided into many sub-jets may make it more easy to study minijets and $E_\perp$-flow, and to interpret the results of the calculations.

- The fact that there are fewer gluons in the primary chain also implies that typical z-values are smaller, and therefore smaller sub-leading effects are expected.

- The formalism is suitable for MC simulation. Such a program is developed by Lönnblad and Kharraziha [7].

Naturally it is essential to verify that the LDC model also can reproduce experimental data. Preliminary results indicate that the LDC MC indeed is able to successfully describe experimental results, both for the structure functions and for the properties of the final states, for example the production of jets and transverse energy flow [8].

4 Integral equations and asymptotic behavior

It is straight forward to derive integral equations for the non-integrated structure function $\mathcal{F}$. From the relation in eq. (12) we obtain the equation

$$\frac{\partial \mathcal{F}(l,\kappa)}{\partial l} = \int_{\kappa_0}^{\kappa} d\kappa' \bar{\alpha}(\kappa) \mathcal{F}(l,\kappa') + \int_{\kappa} d\kappa' \bar{\alpha}(\kappa') \mathcal{F}(l+\kappa-\kappa',\kappa') exp[-(\kappa'-\kappa)] \tag{13}$$

where $l \equiv \ln(1/x)$ and $\kappa \equiv \ln k_\perp^2$.

It is well known that the BFKL formalism with a constant coupling, α_s, implies that the transverse momenta grow like a random walk in $\ln k_\perp^2$, which gives a Gaussian distribution that widens with $\ln(1/x)$, $<\ln k_\perp^2> \sim \sqrt{\ln(1/x)}$. A running coupling favors smaller $k_\perp$-values, and this implies that the $k_\perp$-distribution does not widen indefinitely, but saturates for small x [4]. The solution to eq. (13) can then be written in the factorized form

$$\mathcal{F} \approx \frac{1}{x^\lambda} \cdot f(\kappa), \quad x \text{ small.} \tag{14}$$

The fact that small $k_\perp$-values are not suppressed implies that the evolution and the value of λ is sensitive to the soft region, and therefore cannot be determined from perturbative QCD alone. (This feature is consistent with the very large lower order corrections to the BFKL equation [9], which indicates that the perturbative series may converge badly.) This implies that some kind of cutoff, Q_0, has to be introduced, and determined from fits to experimental data. If this cutoff is determined from fits to data on F_2 from DIS, then this result can be used in our calculation of the minijet distribution in hadronic collisions. Although the dependence on x and $k_\perp$ factorizes as expressed in eq. (14), the two factors are not independent. The relation in eq. (13) implies a correlation such that the power λ also determines the $k_\perp$-dependence. Thus for large $k_\perp$, f takes the asymptotic form

$$f(\kappa) \propto \kappa^{\frac{\alpha_0}{\lambda}-1} \tag{15}$$

where α_0 is defined by the relation

$$\bar{\alpha} \equiv \frac{3\alpha_s}{\pi} \equiv \frac{\alpha_0}{\ln(Q^2/\Lambda^2)} \quad \Rightarrow \quad \alpha_0 = \frac{36}{33 - 2n_f}. \tag{16}$$

Actually MC calculations show that the simple power in eq. (15) is a surprisingly good approximation, not only for large values of $k_\perp$ (or $\kappa = \ln(k_\perp^2/\Lambda^2)$) but for the whole $k_\perp$-interval [4].

The factorized form in eq. (14) implies also, that for limited Q^2 and very small x (or hadronic collisions at very high energies) a central plateau is developed in the minijet distribution. The properties of this plateau will be further studied in the next section.

5 Inclusive Jet Cross Section

In this section we present asymptotic results and general properties. A more detailed analysis will be presented in a future publication.

The properties of the fan diagram in Fig 2 depend on the chosen separation between initial state and final state radiation. As mentioned above, the same event corresponds to a chain with fewer links in the LDC formalism than in e. g. the CCFM formalism, because in the LDC model more emissions are formally treated as final state radiation. The number of jets is not a well-defined concept, if it is not accompanied by some specification of the resolution, and two different schemes can be equally correct if one jet in one scheme corresponds to two or more sub-jets in the other. The total $E_\perp$-flow is however expected to be approximately unaffected, when one jet is split in two or several smaller jets by final state radiation. As mentioned in section 3, the LDC formalism is fully symmetric with respect to the two ends of the fan or ladder diagram, and we will see that this makes it particularly effective for an analysis of the minijet distribution. (In the CCFM formalism the fan diagram for the initial state radiation is not symmetric; the symmetry is restored only after inclusion of the final state emission.) It is also important that the formalism can be interpreted in terms of production probabilities for exclusive final states.

A long chain as in Fig. 5, with a soft probe ($Q^2 \approx Q_0^2$) and with a local maximum $k_{\perp,max} = k_{\perp,i}$, corresponds to a hard scattering between two partons with momenta k_{i-1} and $-k_{i+1}$. Due to the symmetry of the expression in eq. (7), these two pieces of the chain can be interpreted as evolution from both ends towards the central hard scattering. The momentum transfer in this hard subcollision is given by k_i, and there is a minus sign in the momentum of one of the colliding partons, as this part of the chain is regarded as evolving from the top of the fan diagram, downwards towards $-k_{i+1}$.

A single chain may also have more than one local maximum, which corresponds to two or more correlated hard subcollisions. If we want to obtain the inclusive jet cross section, or the total $E_\perp$-flow, we have to include all produced partons q_j in the chain. To calculate this we start by studying a single link in the central part of a long chain. There are three different types of links. Besides a local maximum as in Fig. 5 and Fig. 6a, we have also the two possibilities shown in Fig. 6b and Fig. 6c. To simplify the notation we call the gluons k_a, k, and k_b as indicated in Fig. 6, and study the three cases:

1. $k_\perp > k_{\perp,a}, k_{\perp,b}$. Transverse momentum conservation implies that $q_{\perp,a} \approx q_{\perp,b} \approx k_\perp$, and it corresponds to a normal hard Rutherford scattering between two partons. The two colliding partons have virtualities given by $k_{\perp,a}^2$ and $k_{\perp,b}^2$, which both are

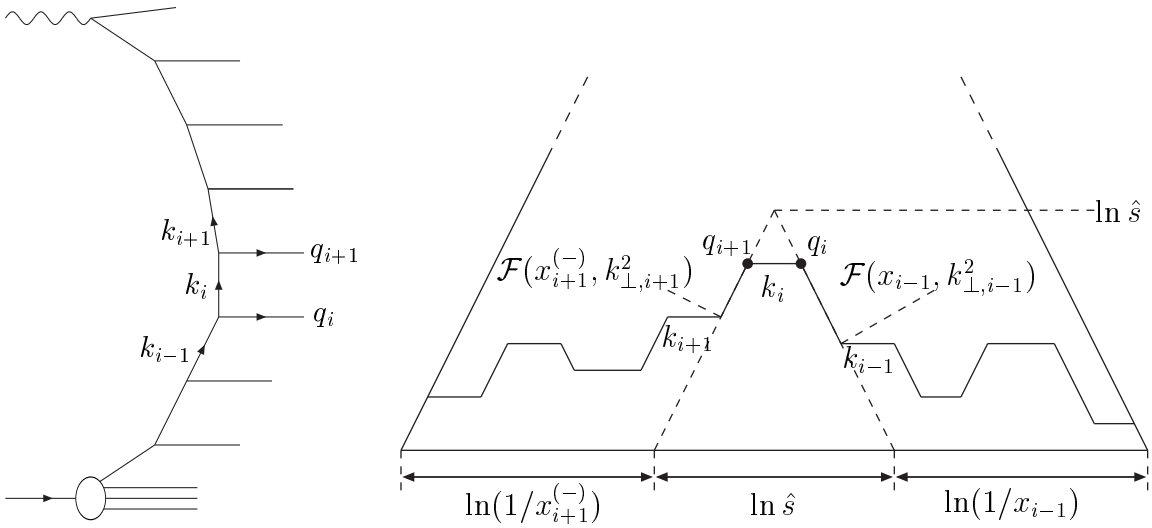

Figure 5: *A local maximum transverse momentum, $k_{\perp,max} = k_{\perp,i}$, in a long chain, corresponds to a hard subcollision between partons with momenta k_{i-1} and $-k_{i+1}$. x_i and $x_i^{(-)}$ are defined as $x_i \equiv k_{+,i}/P_{+,tot}$ and $x_i^{(-)} \equiv -k_{-,i}/P_{-,tot}$ respectively.*

small compared to the exchanged momentum $k_\perp^2$. From eqs. (8-10) we see that the link is associated with the following weight factor

$$\frac{1}{k_\perp^4} \cdot \alpha_s^2(k_\perp^2), \tag{17}$$

which corresponds to the cross section for gluon exchange between two quasireal particles.

2. $k_{\perp,b} > k_\perp > k_{\perp,a}$, which implies that $q_{\perp,a} \approx k_\perp$ and $q_{\perp,b} \approx k_{\perp,b}$. From eq. (9) we see that instead of the expression in eq. (17), this link is associated with the following weight

$$\frac{1}{k_\perp^2 \cdot k_{\perp,b}^2} \cdot \alpha_s(k_\perp^2) \cdot \alpha_s(k_{\perp,b}^2). \tag{18}$$

A similar result is obtained for $k_{\perp,a} > k_\perp > k_{\perp,b}$.

3. $k_\perp < k_{\perp,a}, k_{\perp,b}$, in which case $q_{\perp,a} \approx k_{\perp,a}$ and $q_{\perp,b} \approx k_{\perp,b}$. The corresponding weight is now given by

$$\frac{1}{k_{\perp,a}^2 \cdot k_{\perp,b}^2} \cdot \alpha_s(k_{\perp,a}^2) \cdot \alpha_s(k_{\perp,b}^2). \tag{19}$$

We see that when $k_\perp$ is less than $k_{\perp,a}$ or $k_{\perp,b}$, one factor $1/k_\perp^2$ is replaced by $1/k_{\perp,a}^2$ or $1/k_{\perp,b}^2$ respectively. As will be discussed more in the following, this implies that the inclusive cross section becomes non-singular for small transverse momenta. (As discussed after eq. (12) non-asymptotic contributions to these weights can be included most easily using the MC.)

Keeping k_a, k, and k_b fixed, we note that integrating and summing over all partons to the right of the link corresponds exactly to the non-integrated structure function

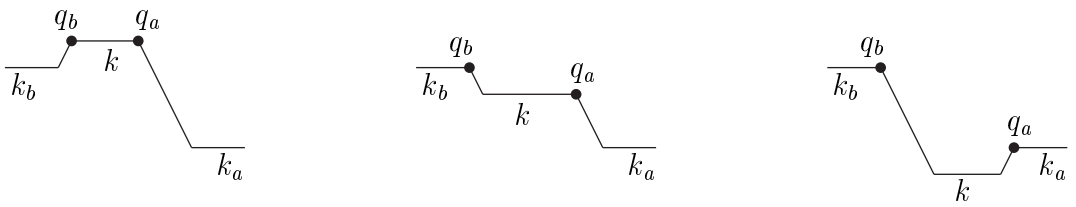

Figure 6: *The three different possibilities for a link.*

$\mathcal{F}(x_a, k^2_{\perp,a})$, where x_a is the Bjorken variable, i. e. the scaled positive lightcone momentum, $x_a = k_{+,a}/P_{+,tot}$. Similarly, integration and summation of partons to the left of the link gives $\mathcal{F}(x_b, k^2_{\perp,b})$, with x_b the corresponding scaled negative lightcone momentum $x_b = x_b^{(-)} = -k_{-,b}/P_{-,tot}$.

The inclusive jet distribution can then be written in the form ($\hat{s}$ is the Mandelstam variable for the hard subcollision)

$$\frac{d\sigma_{incl}}{dq^2_\perp dy} \propto \int \frac{dx_a}{x_a} \cdot \frac{dx_b}{x_b} \cdot \frac{dk^2_{\perp,a}}{k^2_{\perp,a}} \cdot \frac{dk^2_{\perp,b}}{k^2_{\perp,b}} \cdot \mathcal{F}(x_a, k^2_{\perp,a}) \cdot \mathcal{F}(x_b, k^2_{\perp,b}) \cdot \frac{1}{2} \cdot \frac{d\hat{\sigma}}{dq^2_\perp}(q^2_\perp, k^2_{\perp,a}, k^2_{\perp,b}, \hat{s} = x_a x_b s) \cdot \delta(y - \frac{1}{2}\ln\frac{x_a}{x_b}). \tag{20}$$

In this formalism each produced parton is counted in two different links, one to the left and one to the right. In our notation $\frac{d\hat{\sigma}}{dq^2_\perp}$ is the inclusive cross section counting both emitted partons, and therefore a factor $\frac{1}{2}$ is needed to avoid double counting. The cross section $\frac{d\hat{\sigma}}{dq^2_\perp}$ is obtained by integrating eqs. (17-19) over $k^2_\perp$ with the constraint $k^2_\perp < \hat{s}$. In case 1 above we will then get the integral (for $k_{\perp,b} > k_{\perp,a}$)

$$\int_{k^2_{\perp,b}}^{\hat{s}} dk^2_\perp \cdot \frac{1}{k^4_\perp} \cdot 2 \cdot \delta(q^2_\perp - k^2_\perp) = \frac{2}{q^4_\perp} \cdot \theta(q^2_\perp - k^2_{\perp,b}) \cdot \theta(\hat{s} - q^2_\perp). \tag{21}$$

Here the factor 2 in front of the δ-function originates from the fact that we count both $q^2_{\perp,a}$ and $q^2_{\perp,b}$, each being approximately equal to $k^2_\perp$. The contributions from cases 2 and 3 can be calculated in the same way. The result obtained for a running coupling is presented in the appendix. The qualitative features can more easily be understood from the result obtained for a constant α_s, in which case we find (again for $k_{\perp,b} > k_{\perp,a}$)

$$\begin{aligned}\frac{d\hat{\sigma}}{dq^2_\perp} \;\propto\; & \alpha_s^2 \left\{ \frac{2}{q^4_\perp} \cdot \theta(q^2_\perp - k^2_{\perp,b}) \cdot \theta(\hat{s} - q^2_\perp) + \right. \\ & + \frac{1}{q^2_\perp \cdot k^2_{\perp,b}} \cdot \theta(q^2_\perp - k^2_{\perp,a}) \cdot \theta(k^2_{\perp,b} - q^2_\perp) + \delta(q^2_\perp - k^2_{\perp,b}) \cdot \frac{1}{k^2_{\perp,b}} \cdot \ln\frac{k^2_{\perp,b}}{k^2_{\perp,a}} + \\ & + \left. \left[\delta(q^2_\perp - k^2_{\perp,b}) + \delta(q^2_\perp - k^2_{\perp,a})\right] \cdot \left[\frac{1}{k^2_{\perp,b}} - \max\left(\frac{1}{\hat{s}}\,,\, \frac{Q_0^2}{k^2_{\perp,a} k^2_{\perp,b}}\right)\right] \right\}. \end{aligned} \tag{22}$$

Here the first line corresponds to a "normal" hard subcollision, case 1 above. The second line corresponds to case 2, where one of the colliding partons has a virtuality larger than the exchanged momentum $-\hat{t} = k^2_\perp$, and the third line to case 3 where both initial

partons have high virtualities. Note that if we have a soft cutoff Q_0^2, the lower limit in the $k_\perp^2$-integral for case 3 is given by $\max(\frac{k_{\perp,a}^2 k_{\perp,b}^2}{\hat{s}}, Q_0^2)$.

The inclusive jet cross section is now readily obtained from inserting eq. (22) into eq. (20) and integrating with respect to $x_a, x_b, k_{\perp,a}$ and $k_{\perp,b}$. Due to the factorized form $\mathcal{F}(x,\kappa) \approx x^{-\lambda} \cdot f(\kappa)$ in eq. (14), with a power-like dependence on x, the result is independent of the rapidity of the pair, $y = \frac{1}{2}\ln\frac{x_a}{x_b}$, for fixed value of $x_a \cdot x_b = \hat{s}/s$. Thus the distribution corresponds to a central plateau with a height proportional to $(x_1 \cdot x_2)^{-\lambda}$, which for fixed $\hat{s}$ grows with energy proportional to s^λ.

The integration is straight forward if we assume the power-like approximation for $f(\kappa)$ in eqs. (14-15), $\mathcal{F}(x,\kappa) \approx x^{-\lambda} \cdot f(\kappa) \propto x^{-\lambda}\kappa^{\frac{\alpha_0}{\lambda}-1}$. As an example, for the term in eq. (21) (the first term in eq. (22)) the integral over x_a and x_b gives

$$\int \frac{dx_a}{x_a}\frac{dx_b}{x_b}\delta(y - \frac{1}{2}\ln\frac{x_a}{x_b}) \cdot \frac{1}{(x_a x_b)^\lambda} = \int_{q_\perp^2} \frac{d\hat{s}}{\hat{s}} \left(\frac{s}{\hat{s}}\right)^\lambda = \frac{1}{\lambda}\left(\frac{s}{q_\perp^2}\right)^\lambda \tag{23}$$

while the integral over $k_{\perp,a}$ and $k_{\perp,b}$ gives (including also the symmetric case $k_{\perp,a}^2 > k_{\perp,b}^2$)

$$\alpha_s^2(q_\perp^2) \int^{\ln q_\perp^2} d\kappa_b \cdot \kappa_b^{\frac{\alpha_0}{\lambda}-1} \int^{\ln q_\perp^2} d\kappa_a \cdot \kappa_a^{\frac{\alpha_0}{\lambda}-1} = \alpha_s^2(q_\perp^2) \cdot \left[\frac{\lambda}{\alpha_0}\kappa^{\frac{\alpha_0}{\lambda}}\right]^2. \tag{24}$$

The full result for a running coupling, presented in the appendix, is rather lengthy and we write it in the form

$$\frac{d\sigma_{incl}^{jet}}{dq_\perp^2 dy} \propto \frac{s^\lambda}{q_\perp^{4+2\lambda}} \cdot \alpha_s^2(q_\perp^2) \cdot h(q_\perp^2). \tag{25}$$

The factor $s^\lambda/q_\perp^{2\lambda}$ is a consequence of the increase of $\mathcal{F} \sim x^{-\lambda}$ for small x (cf eq. (14)), and we have also extracted a factor $\alpha_s^2(q_\perp^2)$. Thus the function $h(q_\perp^2)$ is defined in such a way, that it would be constant in the unrealistic case, where the parton flux is given by a scaling function $F(x) \sim 1/x^\lambda$, which is independent of Q^2. The result in eq. (25) is proportional to s^λ, but we emphasize that this is the growth of the cross section for jet production, and not the number of jets per event.

Results

For a quantitative estimate of the jet cross section and a comparison with the "naive" approach, it would be suitable to use a Monte Carlo, which can take into account also effects from non-asymptotic energy, non-leading terms in the parton-parton cross section and contributions from quarks. However, we believe that the qualitative features can be understood from an approximate analytic calculation, provided the same approximations are used in both approaches. Thus for $F(x,q_\perp^2)$ and $\mathcal{F}(x,k_\perp^2)$ we use the relations in eq. (12) and eqs. (14-15). We study purely gluonic chains and for the subcollision we use the leading expression $\frac{d\hat{\sigma}}{dq_\perp^2} \propto \frac{\alpha_s^2(q_\perp^2)}{q_\perp^4}$. For the parameters λ and Q_0 (the cut-off for small $k_\perp$) we use the values 0.3 and 0.6 GeV/c respectively, obtained from the MC fit to HERA data. Since we study purely gluonic chains, we may take $n_f = 0$, which implies that the power $\frac{\alpha_0}{\lambda} - 1$ in eq. (15) is close to 2. The result, presented in the appendix, can be written in terms of simple elementary functions when this power is an integer. Numerical calculations show that the result is insensitive to the exact value of the power, and that

the result using $\frac{\alpha_0}{\lambda} - 1 \approx 2$ agrees well with results from the MC. For these reasons we use this value in the results below, and thus assume the following form:

$$\mathcal{F}(x,\kappa) \propto x^{-\lambda} \cdot \kappa^2 \tag{26}$$

which implies that the integrated structure function has the form

$$F(x,\kappa = \ln Q^2) \propto x^{-\lambda} \cdot \left[\frac{1}{3}(\kappa^3 - \kappa_0^3) + \frac{\kappa}{(\lambda+1)^2} + \frac{\kappa^2}{(\lambda+1)}\right] \tag{27}$$

(Note that with our convention $F(x)$ describes the density in $\ln x$, and thus corresponds to F_2. Since we have a hard interaction probe we have included the running of α_s in the final vertex, which implies an extra factor $\ln Q^2 / \ln k_\perp^2$ in the last term in eq. (12).)

The transverse momentum dependence of the function $h(q_\perp^2)$ for a running α_s is shown by the solid line in Fig. 7. Also shown in this figure is the contribution from "normal hard subcollisions", i. e. partons associated to a local maximum in the $k_\perp$ chain. We see that this contribution dominates for large $q_\perp^2$, while for smaller $q_\perp^2$, the partons which are not associated to a local maximum play a more important role, contributing more than 40% for $q_\perp^2 < 5\,\mathrm{GeV}^2$. For large $q_\perp^2$, $h(q_\perp^2)$ behaves as a power of $\ln q_\perp^2$, which corresponds to the scaling violation in the structure functions. For smaller $q_\perp^2$, $h(q_\perp^2)$ is essentially linear in $q_\perp^2$. This implies that the total transverse energy flow $dE_\perp/dy = \frac{1}{\sigma_{tot}} \cdot \int \frac{d\sigma}{dq_\perp^2 dy} dq_\perp^2 \cdot q_\perp$ is convergent for small $q_\perp$ (for $\lambda < 0.5$). Consequently the $E_\perp$ distribution is limited also without a low $q_\perp$ cutoff. In Fig. 7a we also show the $q_\perp$-dependence obtained from the MC (normalized to the same total flow), and, as mentioned above, we see a very nice agreement with our analytic result.

We note that although "normal hard collisions" dominate for large $q_\perp$, the other contributions correspond to approximately 25% even for $q_\perp^2 \approx 1000\,\mathrm{GeV}^2$. We expect that most of this difference would be accounted for in a calculation where hard collisions are calculated to next-to-leading order, including also $2 \to 3$ parton reactions, which thus can take into account one extra parton. This approach would, however not solve the problems encountered for small or medium $q_\perp$.

In the literature the inclusive jet cross section is often estimated from a product of two (integrated) structure functions $F(x,q_\perp^2)$ and a hard subcollision cross section $\frac{d\hat{\sigma}}{dq_\perp^2}$ for quasireal colliding partons. This estimate can be written in the form

$$\begin{aligned}\frac{d\sigma_{incl}^{jet}}{dq_\perp^2 dy} &\propto \int \frac{dx_a}{x_a}\frac{dx_b}{x_b}\delta(y - \frac{1}{2}\ln\frac{x_a}{x_b}) \cdot F(x_a,q_\perp^2) \cdot F(x_b,q_\perp^2) \cdot \frac{1}{q_\perp^4} \cdot \alpha_s^2(q_\perp^2) \propto \\ &\propto \frac{1}{q_\perp^{4+2\lambda}} \cdot \alpha_s^2(q_\perp^2) \cdot h_{naive}(q_\perp^2).\end{aligned} \tag{28}$$

Here the function h_{naive} is defined analogously to the function h in eq. (25).

It is interesting to compare this "naive" estimate with our result in eq. (25). The relation between $F(x,q_\perp^2)$ and the non-integrated structure function $\mathcal{F}(x,k_\perp^2)$ is shown in eq. (12). There are two contributions to F, one (ordered) contribution with $q_\perp > k_\perp$, and another suppressed contribution with $q_\perp < k_\perp$. When one or both colliding partons are virtual, there is a suppression factor $q_\perp^2/k_{\perp,a}^2$ and/or $q_\perp^2/k_{\perp,b}^2$. With a cross section assumed to be proportional to $\frac{\alpha_s^2(q_\perp^2)}{q_\perp^4}$ as in eq. (25), we see that each link is given just the weight presented in eq. (17), eq. (18), or eq. (19). The difference lies in the fact

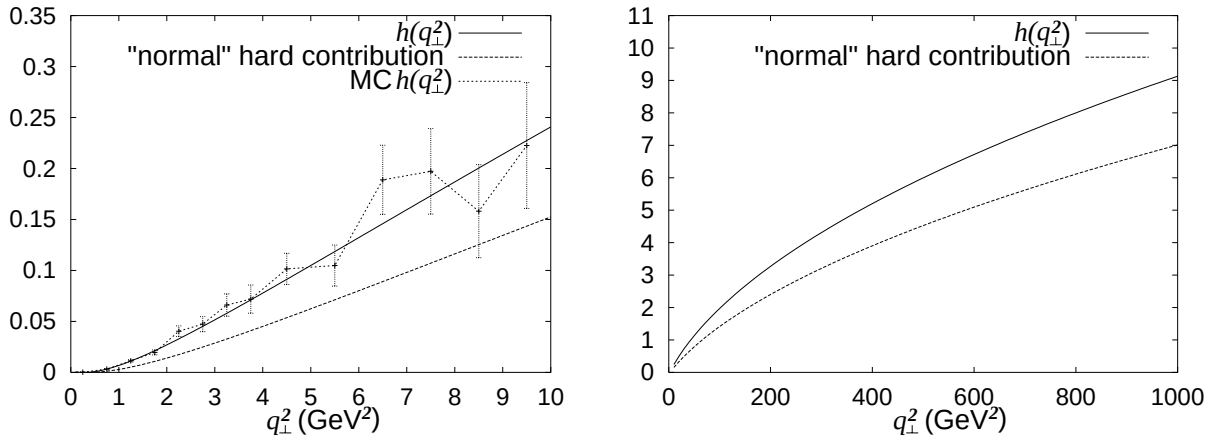

Figure 7: *The transverse momentum distribution of $h(q_\perp^2)$ for (a) $q_\perp^2 < 10$ GeV^2 and (b)$q_\perp^2 < 1000$ GeV^2 according to analytical calculations (continuous curves) and MC simulation (short-dashed line). (The error bars are the estimated statistical uncertainties.) Also shown is the contribution from "normal hard subcollisions" (long-dashed line). The scale is arbitrary.*

that in eq. (28) both outgoing partons are assumed to have transverse momenta given by the momentum transfer in the collision. This underestimates the $q_\perp$ for collisions corresponding to the links in Fig. 6b and Fig. 6c. This underestimate is compensated by the fact that every link in the fan diagram corresponds to a hard collision in eq. (28). Thus this equation corresponds to two produced partons per link instead of one. This double counting does not give a full factor of two, however, due to the underestimate of the $q_\perp$ mentioned above. The result is illustrated in Fig. 8. The really emitted partons in a chain are marked by a dot, while the naive expression in eq. (28) corresponds to a final state parton at every point marked by a circle. Thus in the naive calculation only the partons at a local maximum are given their proper weight. Those at a minimum value for $k_\perp$ should not be included at all, as no real emitted partons have these $k_\perp$-values, and those in-between are counted twice.

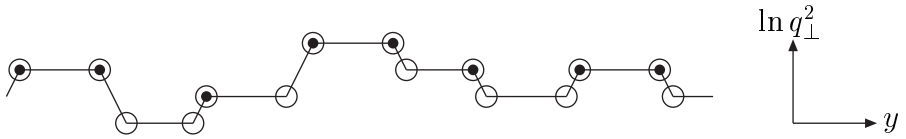

Figure 8: *The outgoing partons according to a correct formalism (dots) and according to a naive approach (circles).*

Fig. 9 shows the ratio $h(q_\perp^2)/h_{naive}(q_\perp^2)$ as a function of the transverse momentum (note the logarithmic $q_\perp$-scale). For large $q_\perp$ the Rutherford contribution dominates in both cases, making $h(q_\perp^2) \approx h_{naive}(q_\perp^2)$. For smaller $q_\perp$, on the other hand, the naive expectation gives a significant overestimate. This can also be concluded from Fig. 10, which shows the distribution in transverse energy, $dE_\perp/dydq_\perp^2 = q_\perp \cdot dn/dydq_\perp^2$. We see that the total $E_\perp$ in the minijet region, $q_\perp \lesssim 5$ GeV, is almost a factor 2 larger in the naive estimate. It is often realized that this large contribution for very low $q_\perp$ must be

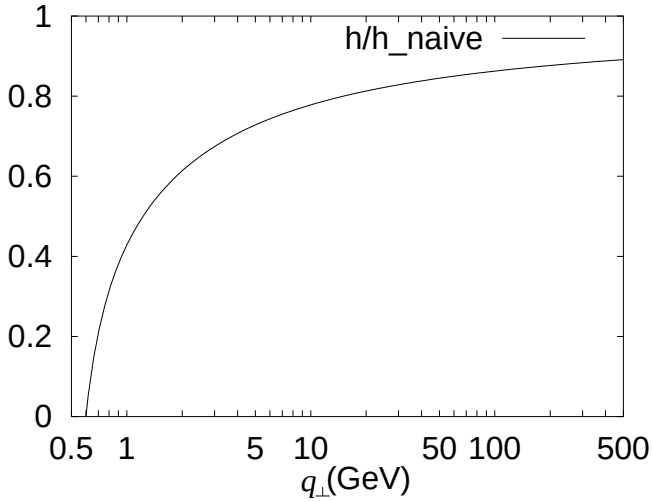

Figure 9: *The ratio $h(q_\perp^2)/h_{naive}(q_\perp^2)$ between the cross section in our approach and the naive expectation in eq. (28), as a function of $q_\perp$. (Note the logarithmic scale on the x-axis.)*

unphysical, and therefore a soft cutoff, $q_{\perp,min}$, is introduced in many calculations. This cutoff is often assumed to be around 2 GeV and slowly growing with energy (see e.g. [5]). In Fig 11 we show the integrated transverse energy $\int^{q_\perp^2} dq_\perp^2 \frac{dE_\perp}{dydq_\perp^2}$. From this figure we see that

$$\int_{Q_0^2}^{\infty} dq_\perp^2 \left.\frac{dE_\perp}{dydq_\perp^2}\right|_{our\ result} \approx \int_{q_{\perp,min}^2}^{\infty} dq_\perp^2 \left.\frac{dE_\perp}{dydq_\perp^2}\right|_{naive} \tag{29}$$

for $q_{\perp,min} \approx 2.1$ GeV. (Remember that the low $k_\perp$-cutoff Q_0 was given by 0.6 GeV.) This means that for asymptotic energies the total $E_\perp$ in our approach equals the naive result when $q_{\perp,min} \approx 2.1$ GeV. For smaller energies the maximal value of $q_\perp$ is limited, which implies that a somewhat smaller value of $q_{\perp,min}$ is needed. A reliable quantitative estimate would need a calculation which includes quark jets and non-leading contributions, which could be obtained with the help of the MC program. We note in particular that in our approach the corresponding effective cutoff of the naive approach, $q_{\perp,min}$, saturates for very large energies. In the conventional approach it is difficult to make predictions for higher energies without a physical understanding of the energy dependence of $q_{\perp,min}$.

Only for comparison, we have in Fig. 10 also included the distribution one would obtain from eq. (25) if the structure function F were scaling and independent of $q_\perp^2$. (The normalization is adjusted to our result for large momenta.) As is seen, this would give a very much larger (and totally unrealistic) increase for small $q_\perp$.

We end this section by noting that one chain forms a set of correlated jets. The fact that the $k_\perp$-distribution saturates for long chains (cf eq. (14)) implies that not only the $p_\perp$ of the jets, but also their density (the number of jets per unit rapidity) is independent of the length of the chain, i. e. independent of the energy in the collision. The jet density grows because the number of possible chains increases proportional to s^λ. It is also conceivable that the number of chains is not random, but e. g. correlated with the impact parameter, so that central collisions have more and peripheral collisions fewer chains [10]. In this paper we have only studied the average jet multiplicity, and we postpone the study of different types of correlations to future investigations.

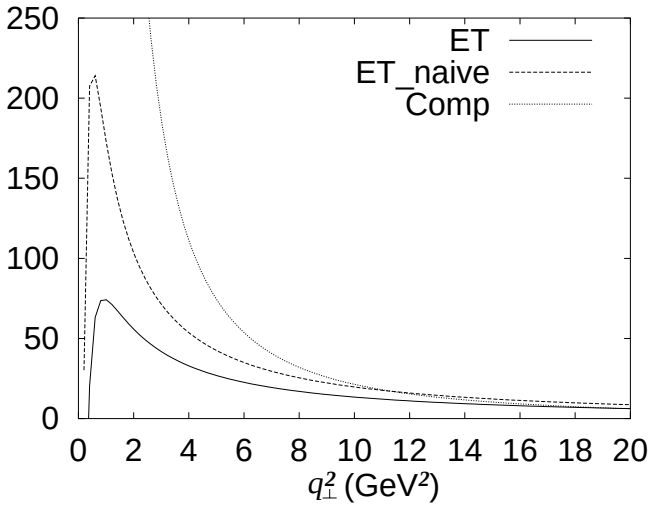

Figure 10: *Transverse energy distribution, $dE_\perp/dydq_\perp^2$, according to our calculations (continuous curve) and the "naive" estimate in eq. (28) (dashed curve). For comparison we also show the result from scaling structure functions, $F(x)$ independent of $q_\perp^2$ (dotted curve). The normalization is arbitrary.*

The possible correlation between different chains may also affect the total cross section. We want to stress that the results in eq. (25) correspond to the cross section for jet production. To find the number of jets per event we have to divide by the total cross section, which is not directly obtained from our formulae.

6 Conclusions

A good understanding of jet and minijet production, and transverse energy flow, is essential for a proper interpretation of new phenomena in pp collisions at LHC or a possible formation of a quark-gluon plasma in nucleus collisions at RHIC or LHC. For very high $p_\perp$ the parton flux can be described by DGLAP ($k_\perp$-ordered) evolution. The large momentum transfer between the colliding partons implies that the two evolving chains are independent of each other. For moderate and smaller $p_\perp$ (and high energies) we enter the BFKL regime and non-ordered chains become important. Here it is essential to take coherence effects and correlations into account. As we can then have several hard subcollisions in a single chain or ladder diagram, it is also important to avoid double counting.

The parton evolution in the BFKL regime can be described e. g. by the CCFM model or the semisoft formalism. The LDC model is a reformulation and generalization of the CCFM formalism, and the symmetric structure of the LDC model makes it particularly suited for a description of (mini)jet production. The result can be interpreted as the production probability for exclusive final states, which makes it convenient for treating the problem of double counting. The (mini)jet cross section is described in a $k_\perp$-factorizing form in terms of non-integrated structure functions and off-shell subcollision cross sections. The result is a dynamical suppression of small-$p_\perp$ jets, which removes the strong sensitivity to a low-$p_\perp$ cutoff in "naive" estimates based on integrated structure functions.

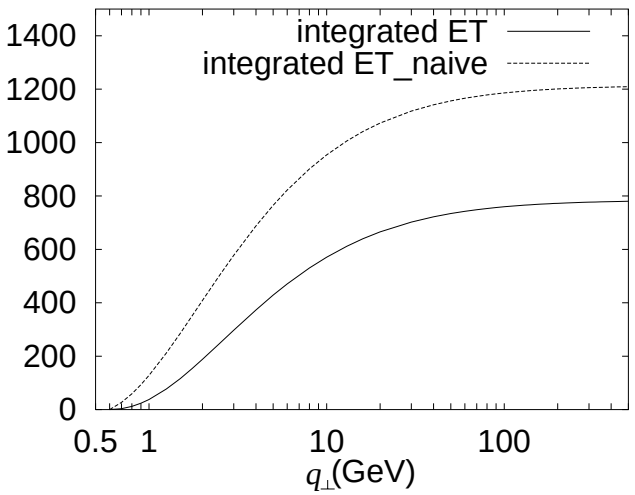

Figure 11: *Integrated transverse energy distribution,* $\int^{q_\perp^2} dq_\perp^2 dE_\perp/dy dq_\perp^2$*, according to our calculations (continuous curve) and the "naive" estimate in eq. (28) (dashed curve). The normalization is as in Fig. 10.*

7 Acknowledgments

We want to thank Bo Andersson and Leif Lönnblad for valuable discussions, and Lönnblad for help with the Monte Carlo simulations.

References

[1] M.Ciafaloni, Nucl.Phys. **B296** (1988) 49;
S.Catani, F.Fiorani and G.Marchesini, Phys.Lett. **B234** (1990) 339; Nucl.Phys. **B336** (1990) 18.

[2] S. Catani, M. Ciafaloni and F. Hautmann, Phys.Lett. **B242**, (1990) 97;
S. Catani, M. Ciafaloni and F. Hautmann, Nucl.Phys. **B366**, (1991) 135;
J. C. Collins and R. K. Ellis, Nucl.Phys. **B360**, (1991) 3;
E. M. Levin, M. G. Ryskin, Y. M. Shabelski and A. G. Shuvaev, Sov.J.Nucl.Phys. **54**, (1991) 867.

[3] B.Andersson, G.Gustafson, J.Samuelsson, Nucl. Phys. **B467** (1996) 443.

[4] B.Andersson, G.Gustafson, H.Kharraziha, Phys.Rev. **D57** (1998) 5543.

[5] T.Sjöstrand, Lund preprint, LUTP 99-42.

[6] E.A.Kuraev, L.N.Lipatov and V.S.Fadin, Zh.Eksp.Teor.Fiz. **72** (1977) 373 [Sov.Phys.JETP **45** (1977) 199];
Ya.Ya. Balitsky and L.N.Lipatov, Yad.Fiz. **28** (1978) 1597 [Sov.J.Nucl.Phys. **28** (1978) 822].

[7] H.Kharraziha and L.Lönnblad, Lund preprint, LUTP 97-34;
H.Kharraziha and L.Lönnblad, JHEP **03** (1998) 006.

[8] H.Jung, L.Lönnblad, Proceedings of the UK Phenomenology Workshop, Durham, Sept. 1999.

[9] V.S.Fadin and L.N.Lipatov, Phys.Lett. **B429** (1998) 127;
G.Camici and M.Ciafaloni, Phys.Lett. **B430** (1998) 349.

[10] T.Sjöstrand and M.van Zijl, Phys.Rev. **D36** (1987) 2019.

8 Appendix

In this appendix we derive the explicit form of the function $h(q_\perp^2)$, which appears in the expression for the total cross section in eq. (25), for the case of a running coupling constant $\alpha_s \propto 1/\ln(k_\perp^2/\Lambda^2) \equiv 1/\kappa$. In each vertex the scale in α_s is taken to be the largest transverse momentum, which due to the consistency constraint in eq. (6) approximately coincides with the largest virtuality. Thus we write the cross section given by eq. (20) in the form

$$\frac{d\sigma_{incl}^{jet}}{dq_\perp^2 dy} \propto \frac{s^\lambda}{q_\perp^{4+2\lambda}} \cdot \alpha_s^2(q_\perp^2) \cdot h(q_\perp^2). \tag{30}$$

As before, we consider separately each of the three possible cases for the relative sizes of the transverse momenta of the gluons k_a, k, and k_b in Fig. 6:

Case 1. $k_\perp > k_{\perp,a}, k_{\perp,b}$, which implies that $q_{\perp,a} \approx q_{\perp,b} \approx k_\perp$,
Case 2. $k_{\perp,b} > k_\perp > k_{\perp,a}$, which implies that $q_{\perp,a} \approx k_\perp$ and $q_{\perp,b} \approx k_{\perp,b}$,
Case 3. $k_\perp < k_{\perp,a}, k_{\perp,b}$, which implies that $q_{\perp,a} \approx k_{\perp,a}$ and $q_{\perp,b} \approx k_{\perp,b}$.

We also assume the power-like approximation for $f(\kappa)$ in eqs. (14-15), $\mathcal{F}(x,\kappa) \approx x^{-\lambda} \cdot f(\kappa) \propto x^{-\lambda}\kappa^{\frac{\alpha_0}{\lambda}-1} \approx x^{-\lambda} \cdot \kappa^2$, where $\frac{\alpha_0}{\lambda} - 1$ is approximately equal to 2.

We start by considering the contribution from case 1. Here the scale in α_s is given just by $k_\perp^2 \approx q_\perp^2$. Thus the only modification to eq. (21) is a factor $\alpha_s^2(q_\perp^2) \propto 1/\ln^2(q_\perp^2)$, which is factored out explicitly in the definition of $h(q_\perp^2)$ in eq. (30). Thus we find

$$\left.\frac{d\hat{\sigma}}{dq_\perp^2}\right|_{contr\ 1} \propto \ 2 \cdot \frac{1}{q_\perp^4} \cdot \frac{1}{\ln^2(q_\perp^2)}. \tag{31}$$

We have a factor 2 in the inclusive cross section, because we count both outgoing partons. When this expression is inserted into eq. (20), the integrations with respect to $k_{\perp,a}$ and $k_{\perp,b}$ give

$$\frac{1}{2}\int_{\kappa_0}^{l_q} d\kappa_b \int_{\kappa_0}^{l_q} d\kappa_a \cdot \frac{2}{q_\perp^4} \cdot \frac{1}{l_q^2} \cdot \kappa_a^2 \cdot \kappa_b^2 = \frac{1}{q_\perp^4} \cdot \frac{1}{l_q^2} \cdot \frac{1}{9} \cdot (l_q^3 - \kappa_0^3)^2 \tag{32}$$

where $l_q \equiv \ln q_\perp^2$ and $\kappa_0 \equiv \ln Q_0^2$. Here the factor $1/2$ compensates for double counting as described in the main text. The remaining integrations with respect to x_a and x_b (cf eq. (23)) give finally:

$$\left.\frac{d\sigma}{dq_\perp^2 dy}\right|_{contr\ 1} \propto \frac{s^\lambda}{q_\perp^{4+2\lambda}} \cdot \frac{1}{l_q^2} \cdot \frac{1}{\lambda} \cdot \frac{1}{9} \cdot (l_q^3 - \kappa_0^3)^2. \tag{33}$$

For case 2, the subcollision cross section $\frac{d\hat{\sigma}}{dq_\perp^2}$ is given by

$$\left.\frac{d\hat{\sigma}}{dq_\perp^2}\right|_{contr\ 2} \propto \int_{k_{\perp,a}^2}^{k_{\perp,b}^2} dk_\perp^2 \cdot [\delta(q_\perp^2 - k_{\perp,b}^2) + \delta(q_\perp^2 - k_\perp^2)] \cdot \frac{1}{k_{\perp,b}^2} \cdot \frac{1}{k_\perp^2} \cdot \frac{1}{\kappa_b} \cdot \frac{1}{\kappa}$$
$$= \frac{1}{k_{\perp,b}^2} \cdot \frac{1}{\kappa_b} \cdot \left[\delta(q_\perp^2 - k_{\perp,b}^2) \ln(\frac{\kappa_b}{\kappa_a}) + \theta(k_{\perp,b}^2 - q_\perp^2)\theta(q_\perp^2 - k_{\perp,a}^2) \cdot \frac{1}{q_\perp^2} \cdot \frac{1}{l_q}\right] \quad (34)$$

After insertion into eq. (20), calculations analogous to the ones in case 1 give the following result for the contribution to the total cross section:

$$\left.\frac{d\sigma}{dq_\perp^2 dy}\right|_{contr\ 2} \propto \frac{s^\lambda}{q_\perp^{4+2\lambda}} \cdot \frac{1}{l_q^2} \cdot \frac{1}{3} \cdot \left\{\frac{1}{\lambda}\left[\frac{l_q^6}{3} - \frac{\kappa_0^3 l_q^3}{3} - \kappa_0^3 l_q^3 \cdot ln\left(\frac{l_q}{\kappa_0}\right)\right] + \right.$$
$$\left. + l_q \cdot (l_q^3 - \kappa_0^3) \cdot \left[\frac{1 + l_q}{\lambda(\lambda+1)} - \frac{1}{(\lambda+1)^2}\right]\right\} \quad (35)$$

In case 3 the appropriate expression for the subcollision cross section $\frac{d\hat{\sigma}}{dq_\perp^2}$ is

$$\left.\frac{d\hat{\sigma}}{dq_\perp^2}\right|_{case\ 3} \propto \int^{k_{\perp,a}^2} dk_\perp^2 \cdot [\delta(q_\perp^2 - k_{\perp,a}^2) + \delta(q_\perp^2 - k_{\perp,b}^2)] \cdot \frac{1}{k_{\perp,b}^2} \cdot \frac{1}{k_{\perp,a}^2} \cdot \frac{1}{\kappa_b} \cdot \frac{1}{\kappa_a}, \quad (36)$$

where the lower integration limit is given by $\max(\frac{k_{\perp,a}^2 k_{\perp,b}^2}{\hat{s}}, Q_0^2)$. Inserting this into eq. (20) and performing the integrations we obtain

$$\left.\frac{d\sigma}{dq_\perp^2 dy}\right|_{contr\ 3} \propto \frac{s^\lambda}{q_\perp^{4+2\lambda}} \cdot \left[\frac{1}{\lambda(\lambda+1)} \cdot l_q \cdot \left(\frac{l_q^2 - \kappa_0^2}{2} + l_q - \kappa_0\right) - \right.$$
$$\left. \frac{1}{(\lambda+1)^2} \cdot l_q \cdot (l_q - \kappa_0)\right]. \quad (37)$$

Adding the three contributions, and including the symmetric situation $k_{\perp,a} > k_{\perp,b}$ to case 2, we find finally for the function $h(q_\perp^2)$ in eq. (30)

$$h(q_\perp^2) \propto \left\{\frac{1}{\lambda} \cdot \frac{1}{9} \cdot (l_q^3 - \kappa_0^3)^2\right\} +$$
$$+ \left\{\frac{1}{\lambda} \cdot \frac{1}{3} \cdot \left[\frac{l_q^6}{3} - \frac{\kappa_0^3 l_q^3}{3} - \kappa_0^3 l_q^3 \cdot ln\left(\frac{l_q}{\kappa_0}\right)\right] + \frac{1}{3} \cdot l_q \cdot (l_q^3 - \kappa_0^3) \cdot \left[\frac{1 + l_q}{\lambda(\lambda+1)} - \frac{1}{(\lambda+1)^2}\right]\right\} +$$
$$+ \left\{\frac{1}{\lambda(\lambda+1)} \cdot l_q^3 \cdot (\frac{l_q^2}{2} - \frac{\kappa_0^2}{2} + l_q - \kappa_0) - \frac{1}{(\lambda+1)^2} \cdot l_q^3 \cdot (l_q - \kappa_0)\right\}. \quad (38)$$

This can be compared with the "naive" expression obtained from eq. (27). With the same normalization we get

$$h_{naive} \propto \frac{2}{\lambda}\left[\frac{1}{3}(l_q^3 - \kappa_0^3) + \frac{l_q}{(\lambda+1)^2} + \frac{l_q^2}{(\lambda+1)}\right]^2, \quad (39)$$

where the factor 2 in the inclusive cross section follows because each hard subcollision produces two jets. We see that the leading term for large $q_\perp$, $\frac{2}{9\lambda}(\ln q_\perp^2)^6$, is the same in both cases, but h_{naive} is significantly larger for smaller $q_\perp$-values.